Materials for Quantum Technology

OPEN ACCESS

RECEIVED
16 July 2025

REVISED
8 October 2025

ACCEPTED FOR PUBLICATION
5 November 2025

PUBLISHED
21 November 2025

LETTER

Deterministic laser-writing of nitrogen-vacancy centres in high purity diamond

Andrew R Kirkpatrick[1,2], Zhin Mai[1], Colin J Stephen[3], Gareth S Jones[1], Gavin W Morley[3], Martin J Booth[2], Patrick S Salter[2] and Jason M Smith[1,*]

[1] Department of Materials, University of Oxford, Oxford OX1 3PH, United Kingdom
[2] Department of Engineering Sciences, University of Oxford, Oxford OX1 3PJ, United Kingdom
[3] Department of Physics, University of Warwick, Coventry CV4 7AL, United Kingdom
[*] Author to whom any correspondence should be addressed.

E-mail: jason.smith@materials.ox.ac.uk

Keywords: diamond, NV centres, laser processing, quantum technology, coherence

Abstract

We report the deterministic writing of single nitrogen-vacancy defects in commercially available high purity diamond using only laser processing. The positioning accuracy of the single defects is around 250 nm and about 20% of the written defects display near transform-limited optical transitions at a temperature of 5 K. The results represent a significant step towards defect-engineered devices using colour centres as coherent spin-photon interfaces for quantum technologies, and shed light on the physical mechanism for laser-induced vacancy diffusion in diamond.

1. Introduction

Colour centre defects in crystalline semiconductors and insulators are at the forefront of developments of quantum networks based on distributed entanglement [1, 2], and offer potential for highly scalable quantum communications and information processing [3]. Among these defects, the negatively charged nitrogen-vacancy centre in diamond (NV^-) currently offers the greatest degree of spin control, with coupling to nearby ^{13}C nuclear spins and to the nuclear spin of the nitrogen atom providing a cluster of high fidelity qubits in which generalised error correction and fault tolerant operations can be performed [4]. The optical transition of the NV^- defect is, however, highly sensitive to the presence of other defects in the surrounding diamond lattice, presenting significant challenges for the high-yield fabrication of NV^- suitable for spin-photon entanglement and the consequent scaling of diamond-based quantum information systems.

The writing of colour centres on-demand at precise locations is a necessary step in the engineering of scalable quantum devices based on these systems. Previously it was shown that deterministic writing of single NV^- defects can be achieved by combining laser-induced vacancy diffusion with fluorescence feedback [5]. In that work a 1 kHz train of laser pulses was used to induce the migration of vacancies to form NV^- centres in a sample containing a nitrogen concentration of 1.8 parts-per-million (ppm). NV^- creation was detected using an *in-situ* confocal fluorescence microscope to monitor the appropriate spectral window and vacancy diffusion was terminated once a stable NV^- signal was detected. Whilst this process was a step forward in NV^- writing, the nitrogen concentration was rather higher than is desirable for prolonged spin coherence, and the diamond sample had been pre-treated using a proprietary method to remove existing NV^- defects. Importantly, the NV^- defects produced did not display coherent optical transitions so would be unsuitable for applications that require spin/photon entanglement.

Here we report the deterministic writing of NV^- defects within commercially available, high purity, diamond. We use single crystal diamond grown by chemical vapour deposition with a nitrogen concentration of < 5 parts-per-billion (ppb) and negligible concentrations of other defects or impurities. By using a pulsed laser with a higher repetition rate and by making other minor modifications to the fabrication process we are able to create single NV^- defects deterministically. The written NV^- defects are found to display coherent optical transitions with a yield of around 20%.

2. Methods

The key challenge in laser writing of NV^- in higher purity diamond is that the laser-generated vacancies must on average travel further during the annealing step before they encounter a nitrogen atom. With [N] < 5 ppb, each vacancy will visit of order 1 million lattice sites on average before an NV^- is formed, compared with of order 1 thousand in the [N] $= 1.8$ ppm diamond used in [5]. Since the laser pulse energy for the annealing step must be kept low enough not to create additional Frenkel defects, a commensurately greater number of pulses is required.

In this work, we use a frequency-doubled Yb:KYW laser (Spectra Physics Spirit), which produces 520 nm, 280 fs laser pulses at a maximum 1 MHz repetition rate. The apparatus is illustrated in figure 1. It consists of two main subsystems; the fabrication system (blue beam path) and a confocal fluorescence microscope (green and red beam paths), used to monitor fluorescence *in-situ* as the annealing is performed.

Power control of the 520 nm writing laser is achieved using a $\lambda/2$ waveplate (Thorlabs WPHSM05-514/WPHSM05-1030) and a Glan-laser polariser (Thorlabs GL5). The beam is then expanded to overfill a spatial light modulator (SLM, dual-band Meadowlark HSP1920-500-1200-HSP8) and then imaged onto the back aperture of an oil immersion objective lens (60X 1.4NA Olympus PlanApo). Aberration correction is performed by the SLM in order to remove both system aberrations and spherical aberrations introduced at the oil/diamond interface.

Fluorescence is excited with a 532 nm CW diode-pumped solid-state laser (Cobalt Samba) with a typical laser power before the objective of 2 mW. The fluorescence excitation laser beam under-fills the objective lens, thereby reducing the effective numerical aperture of the monitor microscope and allowing NV^- formation to be detected over a larger area than that illuminated by the writing laser. A 2-axis galvanometric mirror (Newport FSM-300-01) is used in the fluorescence path, imaged onto the back aperture of the objective with a 4f telecentric lens system, to provide independent positioning of the imaging focal spot in x, y. Fluorescence from the NV^- is collected through the same objective lens and passes back along the green path in figure 1 until being separated from the excitation laser using a 550 nm long-pass dichroic mirror. A further 532 nm notch filter and a 633 nm long pass filter are used to ensure that only NV^- emission is detected. The fluorescence is focused into a fibre-coupled single photon avalanche detector (SPAD) (Excelitas SPCM-AQRH-14-FC), where the fibre aperture is used as the spatial filter for the confocal imaging.

Samples were mounted on a translation stage (Aerotech x–y: ABL10100; z: ANT95-3-V) to provide 3D control of the sample position. Electronic control of the laser fabrication system and confocal microscope was achieved using a field programmable gate array (NI PCI-7830 R) with a user interface written in LabVIEW. Spectroscopy, autocorrelation, power saturation and fabrication accuracy measurements were all performed at room temperature.

Photoluminescence excitation (PLE) characterisation of the zero phonon lines (ZPLs) of the laser-written NV^- defects was performed using a separate microscope incorporating a closed-cycle helium cryostat (Montana S-50) at a temperature of 5 K with an air objective lens (100X 0.9NA Zeiss EC Epiplan-Neofluar). Low temperatures are required for PLE measurements to reduce thermal broadening caused by electron–phonon interaction [6]. The ZPL was resonantly excited by sweeping a tunable diode laser (Newport TLB-6704) across the ZPL emission linewidth, and the resulting photon counts were measured using a SPAD (Excelitas SPCM-AQRH-14). The excitation wavelength was spectrally filtered from the collected photons using a 650 nm long pass filter (Thorlabs FELH0650), and the detuning frequency was measured using a wavemeter (HighFinesse WSU-30). A 532 nm laser (Laser Quantum gem 532) was used for off-resonant repumping of the charge state of the NV^- centre and was pulsed using an acousto-optic modulator (Isomet IMDD-P80L-1.5).

The interaction of femtosecond laser pulses with free carriers during the writing process leads to the generation of a short-lived plasma whose optical emission competes with the NV^- fluorescence at the monitor [7–10]. Figures 2(a) and (b) show, respectively, the spectrum and temporal properties of the plasma emission. In figure 2(a) it can be seen that the plasma emission spectrum overlaps strongly with that of the NV^- figure 4(c), and in figure 2(b) the upper trace reveals that if the SPAD is operated free-running most of the detection events are time-correlated with the writing pulse. In order to prevent this significant background emission from obscuring the creation of an NV^- centre, we therefore time-gate the SPAD to record only between the laser pulses when the plasma emission is absent. The time sequence of this gating is illustrated in figure 2(c).

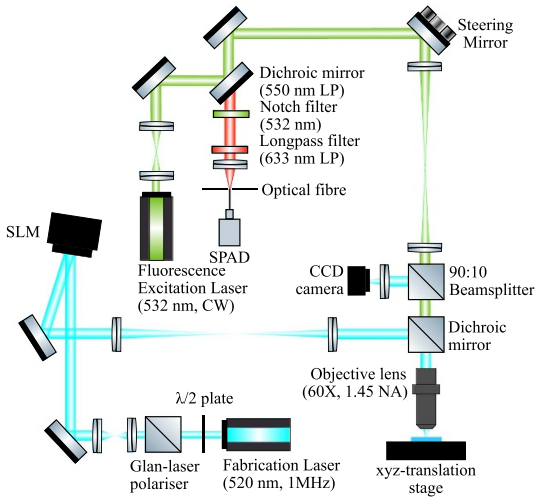

Figure 1. Schematic diagram of the home-built laser fabrication system. This can be separated into two subsystems. Firstly, a fabrication system for SLM assisted fabrication using 520 nm frequency doubled Yb:KYW pulses with a maximum 1 MHz repetition rate, whose beam path is shown in blue. Secondly, a beam-scanning confocal fluorescence microscope which excites with a 532 nm CW laser and monitors the NV^- emission (637–750 nm) using a SPAD. The excitation laser used in this microscope is shown in green and the filtered fluorescence collected by the microscope is shown in red. Each of these subsystems share a common objective lens. Additionally there is a wide-field transmission microscope which contains a CCD camera for sample imaging.

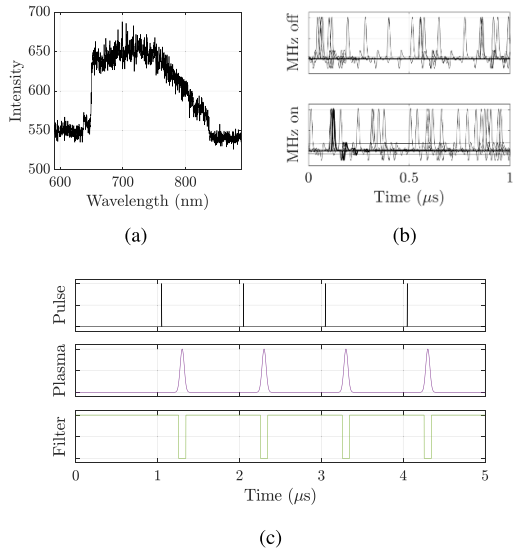

Figure 2. (a) Emission spectrum of the plasma generated during the diffusion process, displaying broadband fluorescence within the NV^- emission window. (b) Timing of recorded SPAD detection events relative to the 1 MHz laser annealing pulses with and without the laser pulse train active. This indicates that when the diffusion pulses are on a large number of detection events occur at 0.1 μs indicating photons generated by the plasma. (c) A pulse train scheme showing how the plasma emission can be temporally filtered by gating the detector off during the plasma emission window.

A single laser pulse is used to generate Frenkel defects in the diamond. The creation of neutral vacancies is signalled by the appearance of weak GR1 fluorescence with a spectral peak at 741 nm [11–13], as shown in figure 3(b). The intensity of this signal indicates the number of neutral vacancies created and is highly sensitive to the laser pulse energy: for this work a seed pulse energy of 1.65 nJ was used.

Following the generation of vacancies, the laser pulse energy is reduced to typically 80% of the seed pulse energy and a train of pulses is delivered at a 1 MHz repetition rate to diffuse the vacancies and produce NV^- centres. The annealing pulse energy is calibrated empirically *in-situ* by starting with a low energy and gradually increasing until the GR1 signal intensity begins to reduce (figure 3(d)), indicating the recombination of some of the Frenkel defects generated by the seed pulse.

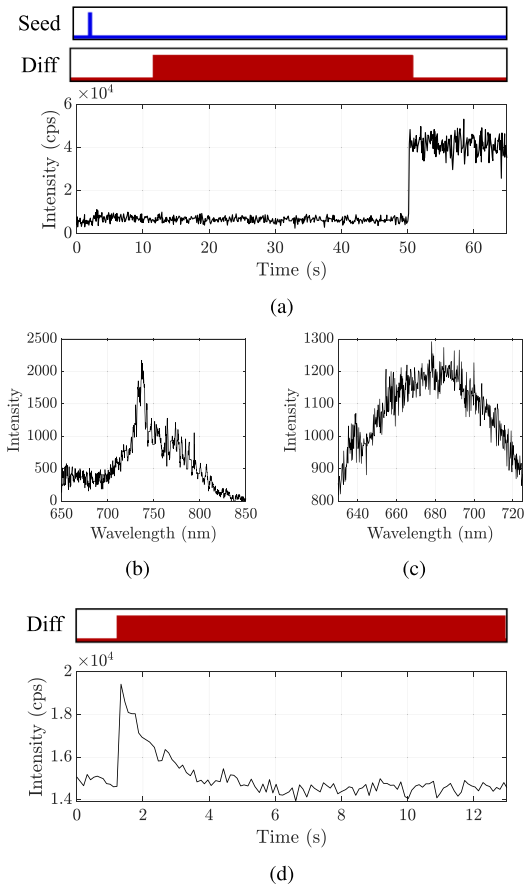

Figure 3. (a) Typical detector trace of the NV$^-$ fabrication process. The blue pulse chart above the traces indicates when the seed pulse occurs. The red pulse charts indicate when the diffusion pulse train is active. (b) Spectral feature indicating the generation of isolated vacancies after the seed pulse and (c) the characteristic NV$^-$ spectral feature measured after the jump in the detector trace at 50 s. (d) Shows the decay over time of the fluorescence from the neutral vacancy during the diffusion process.

The generation of an NV$^-$ centre as annealing progresses is heralded by a sharp step in intensity on the fluorescence monitor (see figure 3(a)). In the majority of cases this fluorescence remains stable after the pulse train has stopped. Spectroscopic analysis of the fluorescence confirms the creation of an NV$^-$ centre, as shown in figure 3(c).

Note that, in contrast with the deterministic laser writing of diamond with higher nitrogen concentration [5], the appearance of stable NV$^-$ fluorescence in the higher purity material is not preceded by an intermittent fluorescence signal. The intermittency observed in the lower purity material is though to be caused by the presence of nearby carbon self-interstitials [14], and so the lack of unstable NV$^-$ emission in the higher purity diamond can be interpreted as a natural consequence of the larger number of anneal pulses required, such that the average separation between as-created NV$^-$ centres and any remaining carbon self-interstitials is much larger.

3. Results

Figure 4(a) shows a 3x3 array of NV$^-$ sites processed using this method, ceasing the anneal pulses upon the appearance of stable NV$^-$ fluorescence. The laser pulses were focused at a depth of 20 μm with a 3 μm separation in$x$–y. 'A depth of 20 μm was chosen out of convenience in order to minimise boiling and lensing effects in the immersion oil during diffusion.'. Eight of the nine sites are found to have a single NV$^-$ defect with clear photon anti-bunching observed in the fluorescence (figure 4(c)). A histogram of the extracted $g^{(2)}(0)$ values is shown in figure 4(d).

One site in the array displays no NV$^-$ fluorescence suggesting that, between fabrication and characterisation, the written defect has either switched charge state or has been destroyed by a nearby interstitial. One possible source of charge state instability is the presence of nearby vacancy aggregates which could be created during the seed or diffusion process. The simplest of these structures, the divacancy, has been shown to be highly stable [15] and may act as a charge trap for the NV$^-$ centre. Divacancies

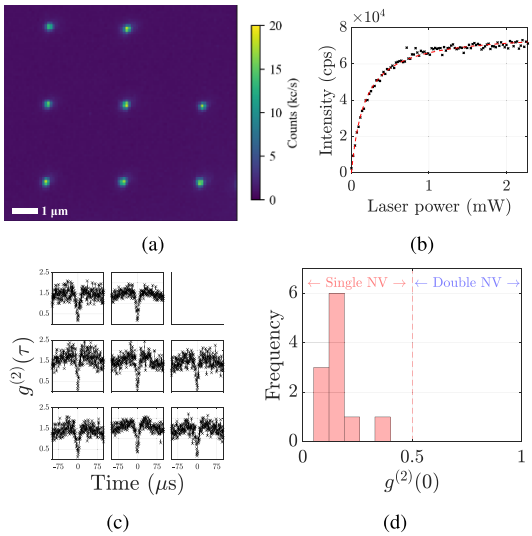

Figure 4. (a) Confocal fluorescence microscopy image of a regular array of NV^- centres created by the laser writing in high purity diamond. (b) A typical power saturation measurement for a single NV^- centre. This behaviour was fit to the function $I(P) = I_\infty \frac{P}{P+P_{sat}}$, where I_∞ and P_{sat} are fitting parameters. (c) Corresponding photon correlation histograms of the array recorded with a Hanbury Brown and Twiss measurement. (d) Histogram of $g^{(2)}(0)$ values confirming that all eight defects in the array are single NV^- centres. Additional data points from NV centres written outside of this array have been included to build statistics.

can be removed by thermal annealing at high temperatures, but it is not currently known whether laser diffusion is capable of dissociating these aggregates.

Figure 4(b) shows a typical power saturation curve for a laser-written NV^- centre. The data collected were fitted to the power saturation equation:

$$I(P) = I_\infty \frac{P}{P + P_{sat}} \tag{1}$$

where I_∞ and P_{sat} are fitting parameters. Typical values for I_∞ and P_{sat} were 7×10^4 s^{-1} and 1.6 mW respectively.

Figure 5 shows PLE spectra of two of the NV^- defects, displaying single scan linewidths of 77.8 ± 5.1 MHz and 34.7 ± 2.3 MHz. These line widths are within a factor of ten of the Fourier transform limit for NV^- demonstrating sufficient coherence for spin-photon entanglement [16]. Figure 5(c) shows a histogram of the measured ZPL line widths from the array.

Figure 6 reports the $x-y$ and z fabrication precision collected from the eight array members and six additional centres fabricated outside of the array ($N = 14$). The $x-y$ positioning accuracy is obtained by fitting a 2D Gaussian function to the measured distribution, which yields a HWHM of 249 ± 35 nm. The z positioning accuracy is obtained by fitting a 1D Gaussian function, which yields a HWHM of 260 ± 80 nm. The positioning accuracy recorded here is significantly lower than that reported previously with laser annealing in [5] and is similar to that produced by thermal annealing in high purity material [17], suggesting that it is determined primarily by the nitrogen concentration of the sample.

This point can be substantiated by considering the mean distance, $\langle r \rangle$, between substitutional nitrogen atoms in the pre-processed diamond:

$$\langle r \rangle \sim \frac{1}{\sqrt[3]{n}} \tag{2}$$

where n is the density of substitutional nitrogen. In the [N] = 1 ppb diamond used here this equates to a mean separation of 178 nm, while in the [N] = 1.8 ppm diamond of [5] the mean separation is 22 nm. The HWHM of the distribution of vacancies produced by the seed pulse has been shown to be less than 50 nm [18], which suggests that the vacancy distribution spreads out during the laser annealing process until a nitrogen atom is 'found'. Previous calculations [18] concluded that the maximum lattice temperature achieved during the seed pulse is about 750 K, insufficient to activate vacancy diffusion. That the anneal pulses are lower in energy provides strong evidence that the annealing mechanism is not thermal in nature. We therefore propose that the vacancy diffusion is induced by excitons which diffuse out from

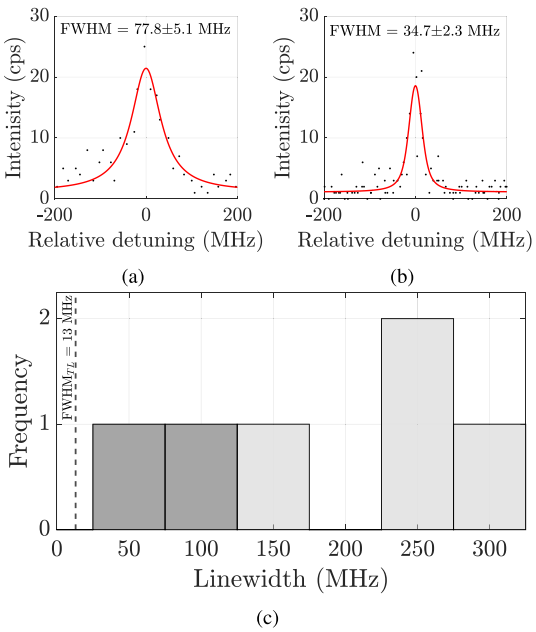

Figure 5. Single sweep PLE spectra of the ZPLs of two different NV^- centres at 5 K, revealing linewidths of 77.8 ± 5.1 MHz and 34.7 ± 2.3 MHz. The FWHMs of the Lorentzian peak fits are indicated at the top left of each graph. (c) Histogram of the measured ZPL linewidths, averaged over multiple laser sweeps, of the NV^- centres created in the array. The 13 MHz transform-limited linewidth has been indicated and the bins corresponding to coherent NV^- centres (< 100 MHz) have been highlighted.

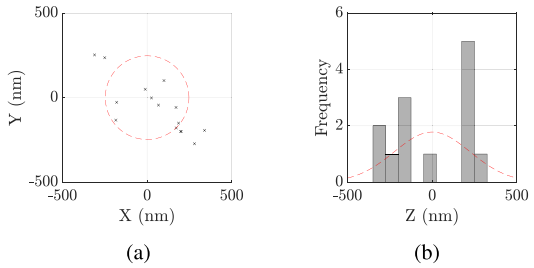

Figure 6. Distributions in (a) *x*–*y* and (b) *z* of the measured positions of the single NV^- relative to the targeted location. The HWHMs of the fitted distribution functions give an *x*–*y* positioning accuracy of 249 ± 35 nm, and z positioning accuracy of 260 ± 80 nm.

the focal spot subsequent to the pulsed excitation and are trapped by vacancies before recombining non-radiatively. Each exciton can provide up to 5 eV of energy, more than sufficient to overcome the vacancy hopping barrier of 2.0 eV. Consequentially, the annealing range is determined by the exciton diffusion length, which in pure diamond is some 50 μm.

4. Conclusion

In conclusion, we report the deterministic writing of single NV^- centres with coherent optical transitions in high purity diamond using laser processing. This is a significant step forward for the realisation of NV^- based devices for quantum communications and computing. The NV^- positioning accuracy achieved using laser annealing in high purity diamond is around 250 nm, suggesting that the process is exciton-mediated.

Data availability statement

All data that support the findings of this study are included within the article (and any supplementary files).

Acknowledgment

The authors acknowledge funding and support from the EPSRC through the DIATOM project (EP/R004803/1), the EPSRC Centre for Doctoral Training in Diamond Science and Technology (EP/L015315/1) and the EPSRC Hub for Quantum Computing and Simulation (EP/T001062/1).

ORCID iDs

Zhin Mai 0009-0005-3892-3809
Colin J Stephen 0000-0003-1734-3571
Gareth S Jones 0000-0003-4302-4101
Gavin W Morley 0000-0002-8760-6907
Jason M Smith 0000-0002-4572-0867

References

[1] Childress L and Hanson R 2013 Diamond NV centers for quantum computing and quantum networks *MRS Bull.* **38** 134–8
[2] Sipahigil A *et al* 2016 An integrated diamond nanophotonics platform for quantum-optical networks *Science* **354** 847–50
[3] Abobeih M H, Wang Y, Randall J, Loenen S J H, Bradley C E, Markham M, Twitchen D J, Terhal B M and Taminiau T H 2022 Fault-tolerant operation of a logical qubit in a diamond quantum processor *Nature* **606** 884–9
[4] Taminiau T H, Cramer J, van der Sar T, Dobrovitski V V and Hanson R 2014 Universal control and error correction in multi-qubit spin registers in diamond *Nat. Nanotechnol.* **9** 171–6
[5] Chen Y *et al* 2019 Laser writing of individual nitrogen-vacancy defects in diamond with near-unity yield *Optica* **6** 662
[6] Fu K-M C, Santori C, Barclay P E, Rogers L J, Manson N B and Beausoleil R G 2009 Observation of the dynamic jahn-teller effect in the excited states of nitrogen-vacancy centers in diamond *Phys. Rev. Lett.* **103** 256404
[7] Keldysh L V 1965 Ionization in the field of a strong electromagnetic wave *Sov. Phys.* **20** 1307–14
[8] Kennedy P K 1995 A first-order model for computation of laser-induced breakdown thresholds in ocular and aqueous media: part I-theory *IEEE J. Quantum Electron.* **31** 2241
[9] Apostolova T and Hahn Y 2000 Modeling of laser-induced break- down in dielectrics with subpicosecond pulses *J. Appl. Phys.* **88** 1024
[10] Gattass R R and Mazur E 2008 Femtosecond laser micromachining in transparent materials *Nat. Photon.* **2** 219–25
[11] Coulson C A and Kearsley M J 1957 Colour centres in irradiated diamonds. I *Proc. R. Soc. A* **241** 433
[12] Yamaguchi T 1962 Electronic states of single vacancies in diamond *J. Phys. Soc. Japan* **17** 1359
[13] Coulson C A and Larkins F P 1969 Electronic structure of the neutral isolated divacancy in diamond *J. Phys. Chem. Solids* **30** 1963
[14] Kirkpatrick A R, Chen G, Witkowska H, Brixey J, Green B L, Booth M J, Salter P S and Smith J M 2023 *Ab initio* study of defect interactions between the negatively charged nitrogen vacancy centre and the carbon self-interstitial in diamond *Phil. Trans. R. Soc.* A **382** 20230174
[15] Slepetz B and Kertesz M 2014 Divacancies in diamond: a stepwise formation mechanism *Phys. Chem. Chem. Phys.* **16** 1515–21
[16] Ruf M, IJspeert M, Van Dam S, de Jong N, van den Berg H, Evers G and Hanson R 2019 Optically coherent nitrogen-vacancy centers in micrometer-thin etched diamond membranes *Nano Lett.* **19** 3987–92
[17] Chen Y *et al* 2017 Laser writing of coherent colour centres in diamond *Nat. Photon.* **11** 77–80
[18] Griffiths B *et al* 2021 Microscopic processes during ultrafast laser generation of frenkel defects in diamond *Phys. Rev. B* **104** 174303